THE JOURNAL OF PHYSICAL CHEMISTRY A

ARTICLE

pubs.acs.org/JPCA

Simulated Annealing and Density Functional Theory Calculations of Structural and Energetic Properties of the Ammonium Chloride Clusters $(NH_4Cl)_n$, $(NH_4^+)(NH_4Cl)_n$, and $(Cl^-)(NH_4Cl)_n$, $n = 1-13$

Robert Q. Topper,*[,†] William V. Feldmann,[‡,§] Isaac M. Markus,[†,∥] Denise Bergin,[†] and Paul R. Sweeney[†]

[†]Department of Chemistry, The Cooper Union for the Advancement of Science and Art, 41 Cooper Square, New York, New York 10003, United States

[‡]Department of Chemistry, Medical Technology, and Physics, Monmouth University, West Long Branch, New Jersey 07764-1898, United States

Supporting Information

ABSTRACT: Simulated annealing Monte Carlo conformer searches using the "mag-walking" algorithm are employed to locate the global minima of molecular clusters of ammonium chloride of the types $(NH_4Cl)_n$, $(NH_4^+)(NH_4Cl)_n$ and $(Cl^-)(NH_4Cl)_n$ with $n = 1-13$. The M06-2X density functional theory method is used to refine and predict the structures, energies, and thermodynamic properties of the neutral, cation, and anion clusters. For selected small clusters, the resulting structures are compared to those obtained from a variety of models and basis sets, including RI-MP2 and B3LYP calculations. M06-2X calculations predict enhanced stability of the $(NH_4^+)(NH_4Cl)_n$ clusters when $n = 3$, 6, 8, and 13. This prediction corresponds favorably to anomalies previously observed in thermospray mass spectroscopy experiments. The $(NH_4Cl)_n$ clusters show alternations in stability between even and odd values of n. Clusters of the type $(Cl^-)(NH_4Cl)_n$ display a magic number distribution different from that of the cation clusters, with enhanced stability predicted for $n = 2$, 6, and 11. None of the observed cluster structures resemble the room-temperature CsCl structure of $NH_4Cl(s)$, which is consistent with previous work. Numerous clusters have structures reminiscent of the higher-temperature, rock-salt phase of the solid ammonium halides.

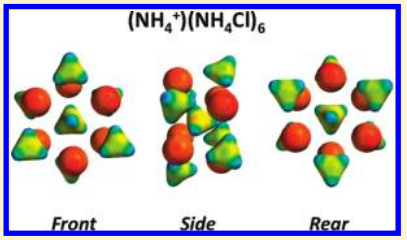

INTRODUCTION

In the present study, we consider the size-dependent structural transitions of ammonium chloride clusters as they grow to larger size. At some critical size, the energetically favored structures of such particles should resemble those observed in the bulk.[1,2] Yet precisely how large must a salt particle become for its properties to resemble those of the bulk? There is then the possibility that smaller particles have unique chemical or physical properties. For example, does a dry cluster of ammonium chloride have the same acidic corrosivity that is exhibited by the bulk material, or is its nature dependent on particle size?[3] Moreover, the clusters can be formed as subunits of a larger molecule. Recently, a cubic tetramer cluster, that is, $(NH_4Cl)_4$, was synthesized at the core of a cluster compound, that is, at the center of the dimer of *N*,*N*-bis(3-amino-3,3-diallylpropyl)-4-methylbenzolsulfonamide dihydrochloride.[4] It may be that even larger cluster compounds are synthetically accessible.

The size-dependent energetics of ammonium chloride particles are relevant to the study of atmospheric aerosols in polluted marine environments.[5] Harrison and Pio reported that the atmospheric ammonium chloride particles that may be found in polluted atmospheres are typically in the submicrometer size range.[6] Under certain conditions, ammonium nitrates and chlorides can make up a sizable mass percentage of the aerosol mass. The particle size distribution must be known, or assumed, to accurately model the aerosol growth kinetics.[7−11] Thermospray mass spectrometry (TS-MS) has been used by Röllgren and co-workers to study the particle size distribution for $(NH_4^+)(NH_4Cl)_n$ clusters with $n \leq 13$.[12,13] Their work shows magic numbers, that is, clusters with notable relative stability, for $n = 3$, 6, and 13. Two anomalies were observed. First, the $n = 2$ cluster is not present in the mass spectra, whereas for alkali halide cluster systems, $n = 2$ is a prominent peak. Second, the relative intensities for the $n = 4$, 5, and 6 clusters are reversed; that is, for the ammonium halide clusters, $I(n = 4) < I(5) < I(6)$, but the reverse is true for $Cs^+(CsCl)_n$ clusters. In the present work, we are, within limits, able to correlate the stability pattern of the cation clusters with the magic number distribution observed with TS-MS as well as interpret these anomalies.

Long-range Coulombic forces presumably dominate the energetic and structural properties of bulk ammonium chloride.[2] However, in clusters, the saturation of attractive N−H···Cl− interactions is also an important factor in determining which structures are favored.[14,15] These same interactions are very important to the phase behavior of the solid state. Below 458 K, solid NH_4Cl has the CsCl crystal motif with each NH_4^+ surrounded by a cubic cage of eight nearest-neighbor Cl^- ions.[16]

Received: July 21, 2011
Published: August 18, 2011

At low temperature (the δ phase), the NH_4^+ ions are oriented so that the tetrahedral ion is coordinated with four of the surrounding Cl^- ions and all NH_4^+ ions are ordered; that is, they have the same orientation as one another throughout the crystal. As the system is warmed to 243 K, the solid exhibits an order−disorder phase transition (with weak first-order character) to the β phase. At room temperature, the NH_4^+ ions are orientationally disordered and are essentially free to rotate within the lattice.[17,18] Each individual ammonium ion must overcome a rotational energy barrier of approximately 18−20 kJ mol^{-1}.[18,19] When the temperature is further increased to 458 K, ammonium chloride undergoes another solid−solid phase transition to the α phase, which has a rocksalt crystal structure analogous to that of NaCl.[16]

In an early theoretical study, the structures and isomeric properties of $(NH_4Cl)_n$ (n = 3−10) clusters were predicted by Matro et al. using simulated annealing Brownian dynamics and "jump-walking" Monte Carlo calculations.[14] An even−odd alternation in the stability of the clusters toward monomer growth was predicted, with the tetramer cluster assuming a cubic structure and having the greatest stability. Even-numbered clusters (as well as n = 9) took on slab-like structures with patterns reminiscent of the "rocksalt" structure observed in bulk NaCl, whereas odd-numbered clusters typically had more compact forms. Several of the odd-numbered clusters (n = 3, 5, and 7) displayed isomerism at moderate temperatures. None of the predicted cluster structures resembled the bulk, CsCl-type structure of room-temperature NH_4Cl (s).

The potential energy model used in the simulations by Matro et al.[14] presumed that the clusters consist of NH_4^+ and Cl^- particles that interact with one another according to an effective pair potential.[18] It was known from previous work that the monomer cluster structure is a van der Waals structure best described as $NH_3\cdots HCl$.[20−22] Subsequent ab initio and density functional theory studies of the neutral $(NH_4Cl)_n$ (n = 1−4) clusters have confirmed that for $n \geq 2$ the cluster structures are ionic, whereas the n = 1 structure is a hydrogen-bonded system.[15,23−26] In all cases, the structures built and studied in these papers for values of $n > 1$ were similar to those that had been predicted by the Monte Carlo and Brownian dynamics simulated annealing calculations.[14] Proton transfer between NH_3 and an acid molecule has been predicted in other neutral cluster systems and appears to occur with as few as one additional molecule in the cluster above the monomer pair.[27,28] In one experiment, proton transfer within the $NH_3\cdots HCl$ monomer cluster was induced by addition of an extra electron.[29] A number of theoretical studies of hydrated ammonium chloride clusters $(NH_3{:}HCl{:}(H_2O)_n$ (n = 0−3)) have been carried out.[30−32] These studies showed that the hydrated monomer clusters must have one or two water molecules for proton transfer between NH_3 and HCl to be observed.

In this work, we present a study of a more extensive size range of the $(NH_4Cl)_n$ clusters than has previously been presented in the literature, as well as what is apparently the first theoretical study of $NH_4^+(NH_4Cl)_n$ and $Cl^-(NH_4Cl)_n$ clusters. Simulated annealing Monte Carlo methods are used to locate the minimum-energy structures, and density functional theory (DFT) calculations using the B3LYP[33,34] and M06-2X[35] methods are then used to refine the resulting structures. M06-2X is a hybrid DFT method developed specifically to yield an improved description of noncovalent interactions.[36] In the case of $[NH_4^+\text{-}(NH_4Cl)_m]$, the variations of the binding energy with n are compared to the "magic numbers" observed through the use of TS-MS, and the results are used to interpret the experimental data.[12] The structural trends are discussed, and the energetics of reactions relevant to the modeling of nucleation and particle growth under dry conditions are also presented.

METHODS

Small $(NH_4Cl)_n$ clusters are predicted to exhibit size-dependent isomeric forms, particularly when n is small and odd.[14] The use of Monte Carlo methods that are both highly ergodic and efficient is important if the goal is to find the minimum-energy structure (or structures) of the system.[37] In the present work, the method chosen for this purpose is known as "mag-walking" (MW).[38,39] When combined with simulated annealing (SA), the method is hereafter referred to as the MW-SA method. We confine the present discussion to an outline of the MW-SA method and the specifics of its application to the present work.

In the current work, several modifications are made to the original Metropolis algorithm.[40] At a specified temperature, a Metropolis Monte Carlo calculation is carried out in which each trial moves the random selection of an ion, followed by a Barker−Watts rotational sample of a molecular orientation[41] and/or a translational move of an atomic ion or a molecular ion's center of mass. The trial move step sizes are optimized so as to accept roughly 50% of the attempted moves. Next, a longer, mag-walking calculation is carried out, in which a probability (usually about 10%) is assigned for any given trial move to be carried out using either the optimized step size or a magnified step size during the random walk. The magnified Barker−Watts rotational step size is chosen so as to allow the molecule to fully rotate around a given axis, whereas the magnified translational stepsize is chosen to be a predetermined multiple of the optimized step size (usually a factor of 10 larger). This method is highly ergodic and obeys the detailed balance condition as well.[39]

To provide the best opportunity for sampling all important structures, simulated annealing is combined with mag-walking. The simulated annealing method for global optimization was introduced by Kirkpatrick et al.[42] In simulated annealing calculations, the simulation temperature is slowly decreased from an initially high value until the system is quenched into a minimum-energy structure. The initial temperature must be sufficiently high to ensure ergodic sampling on the simulation time scale. Ideally each cluster is cooled at an infinitely slow rate, using an exponentially decaying temperature variation to ensure complete quenching.[42] In practice, both of these requirements can be modified, and in previous work we have found that using a "sawtooth" annealing schedule is an efficient route to reproducibly and efficiently finding the minimum-energy structures of small molecular clusters.[43]

All MW-SA calculations are initiated from randomly chosen initial geometries, which are screened to avoid any initial direct overlaps between atoms. Once a suitable initial geometry is found, each system is initially equilibrated for 25 000 or more particle moves, depending on the system. The temperature is then linearly decreased at a slow rate from T_1 to 0 K, and then instantly increased to 80% of T_1 and linearly decreased from 0.80 T_1 to 0 K at 80% of the initial annealing rate. This procedure is repeated for anywhere from 10 to 15 "sawtooth" cycles, depending on what is needed to obtain reproducibility of the results. After the final sawtooth is completed, the cluster is further

annealed for an additional equilibration cycle at 0 K in which only "downhill" Barker−Watts and/or translational moves are accepted, and the mag-walking probability is set equal to zero.

These calculations were repeated with different input conditions and sampling parameters (including the number of Monte Carlo cycles per temperature as well as the number of temperatures and the uppermost temperature) to ensure that the results were not sensitive to any of the input parameters. The MW-SA calculations yielded cluster structures for $(NH_4Cl)_n$ ($n = 2-10$) in excellent agreement with structures predicted previously using independent parallel jump-walking Monte Carlo and simulated annealing Brownian dynamics calculations.[14] By examining the structures at the end of each sawtooth cycle, it is also possible to sometimes identify local minimum-energy structures of interest. In this Article, the focus is on the global minimum-energy structures. The temperature dependence of structural transitions of the neutral clusters has been studied elsewhere.[14]

The interaction potential energy model used in the MW-SA calculations was the same as used in previous work.[14] In all MW-SA calculations, the ammonium ions are held rigid. Relaxing this condition and allowing the ammonium to distort within an internal harmonic force field was previously shown to have only a small quantitative effect on the structures and energies of the annealed clusters.[14]

In the MW-SA calculations, the temperatures are sometimes sufficiently high that ions can evaporate from the cluster during the annealing schedule. This Article's focus is on locating minimum-energy structures rather than attempting to characterize evaporative processes. For this reason, a constraint potential that is only measurable when ions move too far away from the center of the cluster is employed, as suggested by Lee and coworkers.[44] The constraint potential ensures that molecules cannot evaporate from the cluster at the initial, unphysically high temperature of the simulation. As in previous work,[14] the constraint potential is of the form:

$$V_C(r) = \kappa \sum_{i=1}^{n} (|r_i - R_{cm}|/R_c)^{20} \quad (1)$$

where n = the number of ions, R_{cm} is the vector locating the center of mass of the cluster, r_i is a vector locating the center of mass of each ion, R_c is a radial scaling parameter (which ranged from 15.0 to 30.0 Bohr), and κ is an arbitrary constant with units of energy ($\kappa = 1$ hartree in the calculations presented here). The results presented here were found to be insensitive to the specific parameters of the constraint potential as long as the value of R_c was sufficiently large.

Given the size of the largest clusters studied here, carrying out accurate computations of the entire cluster profile for all three systems using a single, consistent quantum mechanics method of sufficiently high accuracy presented challenges. Although for small ammonium chloride clusters it is practical to carry out geometry optimizations using large basis sets, for large clusters one must use a combination of methods and basis sets that are computationally feasible while not sacrificing accuracy.

One expects generally that because the systems consist of ionic particles, the use of diffuse functions will be important in predicting the cluster energies.[45] It has already been shown that large basis sets are necessary to obtain well-converged MP2 geometries for the NH_3---HCl cluster.[15,23] However, all of the other clusters are dominated by ionic interactions (NH_4^+---Cl^-) and may therefore have very different convergence properties.

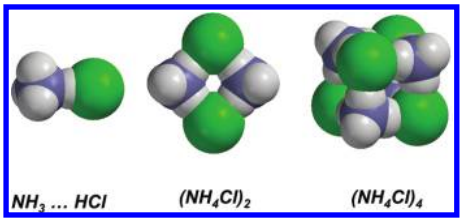

Figure 1. Geometries of $(NH_4Cl)_n$ clusters with $n = 1$, 2, and 4. The $n = 1$ cluster is best described as $NH_3\cdots HCl$, whereas all other clusters are composed of NH_4^+ and Cl^- ions.

In the Results, we compare B3LYP and M06-2X geometries for selected cluster systems ($n = 1$, 2, and 4 neutral clusters) to those variously obtained using the MP2 and RI-MP2 methods.[46] For $n > 1$ clusters, the geometries and zero-point energies using the M06-2X/6-31G(d,p) method are acceptably close to those using much larger basis sets that include diffuse functions. This finding is important to make the problem sufficiently computational tractable to model clusters throughout the size regime accessed via mass spectrometry. With respect to the vibrational frequencies, the monomer cluster has been reported to exhibit significant anharmonicity in the proton-stretching frequency.[23] Harmonic frequencies and structures were observed to be relatively insensitive to the level of theory when the basis set is adequate, but the anharmonic stretch frequency was fairly dependent on whether or not electron correlation was treated adequately.[28] In this Article, zero-point energies are calculated using harmonic frequencies and the 6-31G(d,p) basis set.

Following DFT geometry optimization, a variety of methods and basis sets were used for single-point energy calculations. In one set of calculations, B3LYP/6-31G(d,p) geometry optimizations and frequency calculations were carried out followed by single-point calculations at the B3LYP/6-311G++(2df,2p) level. In another set of calculations, M06-2X/6-31G(d,p) geometry optimizations and frequency calculations were carried out, followed by single-point M06-2X/6-311++G(2df,2p) calculations. A third set of calculations on a subset ($n < 7$) of the cation clusters used M06-2X/6-31G(d,p) geometry optimization and frequency calculation followed by single-point M06-2X/aug-cc-pVTZ calculations.[47] No corrections were made to take basis set superposition error (BSSE) into account. BSSE errors are expected to be on the order of 1 kcal/mol or less, which is small as compared to the interaction energies and reaction enthalpies considered here; BSSE would produce errors that are less than 1%. For this reason, we do not expect the qualitative predictions of these calculations to be altered by the neglect or inclusion of BSSE corrections. In addition, we expect that the use of the M06-2X method together with the inclusion of diffuse functions in the basis set will tend to minimize the magnitude of BSSE.[48,49] All density functional theory and ab initio calculations were variously carried out using GAMESS[50] and the Spartan 08 interface to QChem 3.2.[51] All M06-2X calculations used the SG-1 numerical integration grid and strict convergence criteria to achieve numerical stability in the calculated energies and frequencies. The MW-SA calculations were carried out using ANNIE, an architecture-independent FORTRAN program written by the authors.

RESULTS

To explore the dependence of the predicted cluster geometries on the chosen basis set and method, a series of calculations

Table 1. Experimental and Calculated Atom−Atom Distances for the $H_3N\cdots HCl$ Cluster

method	basis set	r_{NH} (Å)	$r_{N\cdots H}$ (Å)	r_{HCl} (Å)	$r_{N\cdots Cl}$ (Å)	% dev [h]
expt. [a]		NR[i]	NR	NR	3.137	
CCSD(T)	6-311++G(2df,2pd) [b]	1.014	1.831	1.311	3.142	0.2%
CCD	6-311++G(2df,2pd) [b]	1.011	1.873	1.303	3.176	1.2%
MP2	6-311++G(d,p)[b]	1.016	1.818	1.312	3.130	−0.2%
	6-311++G(2d,p)[c]	1.016	1.777	1.322	3.099	−1.2%
	6-311++G(2df,2pd)[b]	1.012	1.760	1.319	3.079	−1.8%
	aug-cc-pVDZ[d]	1.020	1.726	1.343	3.069	−2.2%
	TZP[e]	1.012	1.778	1.321	3.099	−1.2%
RI-MP2	6-31G(d,p)	1.013	1.775	1.316	3.091	−1.5%
	6-31+G(d)	1.019	1.820	1.322	3.142	0.2%
	6-311++G(2df,2p)	1.011	1.742	1.327	3.069	−2.2%
B3LYP	6-31G(d,p)	1.017	1.670	1.361	3.030	−3.4%
	6-31+G(d)[c]	1.019	1.688	1.363	3.051	−2.7%
	6-311+G(d,p)[f]	NR	1.733	1.346	3.079	−1.8%
	6-311++G(d,p)[b]	1.010	1.819	1.325	3.144	0.2%
	6-311++G(2d,p)[c]	1.016	1.733	1.346	3.079	−1.8%
	6-311++G(2df,2pd)	1.013	1.733	1.341	3.075	−2.0%
	cc-pVTZ	1.013	1.738	1.343	3.081	−1.8%
	d-aug-cc-pVDZ[g]	NR	1.672	1.368	3.040	−3.1%
M06-2X	6-31G(d)	1.017	1.633	1.367	3.000	−4.4%
	6-31G(d,p)	1.015	1.628	1.363	2.991	−4.7%
	6-31+G(d)	1.018	1.645	1.363	3.008	−4.1%
	6-311+G(d,p)	1.015	1.686	1.348	3.034	−3.3%
	6-311++G(d,p)	1.015	1.685	1.348	3.033	−3.3%
	6-311++G(2d,p)	1.015	1.690	1.344	3.035	−3.3%
	6-311++G(2df,2pd)	1.013	1.703	1.338	3.041	−3.1%
	cc-pVTZ	1.013	1.715	1.338	3.054	−2.6%
	aug-cc-pVTZ	1.012	1.710	1.340	3.050	−2.8%

[a] Reference 52. [b] Reference 28. [c] Reference 15. [d] Reference 31. [e] Reference 23. [f] Reference 30. [g] Reference 32. [h] Percent deviation from the experimentally determined N---Cl distance. [i] NR = not reported. r_{NH} is the covalent N−H bond distance within the NH_3 molecule, whereas $r_{N\cdots H}$ is the noncovalent distance between N of the NH_3 molecule and H of the HCl molecule.

were made of the $NH_3\cdots HCl$ monomer cluster as well as the $(NH_4Cl)_2$ and $(NH_4Cl)_4$ clusters (Figure 1). The $N\cdots Cl$ distance of the $NH_3\cdots HCl$ cluster was determined experimentally by Goodwin et al.[52] and has also been predicted in a number of theoretical studies. In the absence of more detailed experimental data, this bond distance is used to gauge the quality of each method and basis set. A summary of the performance of a variety of theoretical methods in the prediction of the $N\cdots Cl$ distance for the $NH_3\cdots HCl$ cluster is shown in Table 1. The CCSD(T)/6-311++G(2df,2pd) calculations by Biczysko et al.[28] predicted this distance within 0.2% of the experimental value. MP2 calculations of N---Cl distances yield absolute deviations ranging from 0.2% to 2.2%, depending on the basis set employed. Our M06-2X calculations with various basis sets produce absolute deviations ranging from 2.6% to 4.7%, and the B3LYP absolute deviations range from 0.2% to 3.4%. The situation is substantially different for larger clusters.

The $(NH_4Cl)_2$ dimer cluster exhibits qualitatively different intermolecular forces within the cluster. The neutral dimer is cyclic and is composed of ammonium (NH_4^+) and chloride (Cl^-) ions at all levels of theory and for all basis sets employed. Although the experimental N---Cl distance is not known for the dimer, the quality of the various calculations can be gauged somewhat by comparison to RI-MP2/aug-cc-pVTZ calculations, as well as to MP2/6-311++G(2d,p) calculations presented by Tao[15] and MP2/TZP calculations by Chaban et al.[23] As seen in Table 2, the B3LYP method shows deviations for the dimer cluster, which are similar to those that are seen in the monomer. However, the M06-2X method fares much better, with absolute deviations of the N---Cl distance ranging from 0.0% to 0.8%. This performance is similar to that of the MP2 and RI-MP2 calculations, which range from 0.4% to 2.2% absolute deviations for the smaller basis sets. Looking broadly at all of the geometric parameters, the agreement between the M06-2X/aug-cc-pVTZ and M06-2X/6-31G(d,p) is fairly good, which helps justify the use of the smaller of these two basis sets for the geometries of the clusters.

The $(NH_4Cl)_4$ tetramer cluster, which is a distorted cube,[14] was also studied at various levels of theory and with a variety of basis sets, and the results are shown in Table 3. In this case, the "best" calculation used for comparison is geometry optimization at the RI-MP2/aug-cc-pVTZ level. It can be seen that the M06-2X/6-31(d,p) geometry is in good agreement, with an absolute % deviation of 0.1% of the N---Cl distance from the RI-MP2 result, which is less than 0.01 Å. The use of M06-2X/6-311G++(2df,2p) or M06-2X/aug-cc-pVTZ predicts an N---Cl distance with reliably small

Table 2. Calculated Atom−Atom Distances for the $(NH_4Cl)_2$ Cluster

method	basisSet	r_{NH} in NH_4^+ outside ring (Å)	r_{NH} in NH_4^+ within ring (Å)	$r_{H\cdots Cl}$ (Å)	$r_{N\cdots Cl}$ (Å)	% dev [b,d]
MP2	6-311++G(2d,p)[a]	1.017	1.067	1.944	3.003	0.4%
	TZP[b]	1.014	1.062	1.941	NR	
RI-MP2	6-31G(d,p)	1.015	1.064	1.948	3.004	0.4%
	6-31+G(d)	1.022	1.061	2.004	3.057	2.2%
	6-311++G(2df,2p)	1.013	1.061	1.948	3.003	0.4%
	cc-pVTZ	1.013	1.067	1.917	2.978	−0.4%
	aug-cc-pVTZ	1.014	1.065	1.932	2.991	
B3LYP	6-31G(d,p)	1.019	1.077	1.945	3.015	0.8%
	6-31+G(d)[a]	1.021	1.072	1.978	3.044	1.8%
	6-311+G(d,p)[c]	1.018	1.072	1.961	3.026	1.2%
	6-311++G(2d,p)[a]	1.018	1.073	1.957	3.022	1.0%
	6-311++G(2df,2p)	1.018	1.072	1.963	3.027	1.2%
M06-2X	6-31G(d,p)	1.018	1.076	1.924	2.992	0.0%
	6-31+G(d)	1.020	1.070	1.957	3.019	0.9%
	6-311++G(2df,2p)	1.014	1.071	1.927	2.992	0.0%
	aug-cc-pVTZ	1.014	1.071	1.930	2.995	0.1%

[a] Reference 15. [b] Reference 23. [c] Reference 31. [d] Percent deviation of $r_{N\cdots Cl}$ from the value predicted by RI-MP2/aug-cc-pVTZ. r_{NH} is a covalent N−H bond distance within the NH_4^+ molecule, whereas $r_{X\cdots Cl}$ (X = H or N) is the noncovalent distance between an atom within the NH_4^+ molecule and the nearest-neighbor Cl^-. NR = not reported.

Table 3. Calculated Atom−Atom Distances for the $(NH_4Cl)_4$ Cluster

method	basis	r_{NH} in NH_4^+ outside cube (Å)	r_{NH} in NH_4^+ within cube (Å)	$r_{H\cdots Cl}$ (Å)	$r_{N\cdots Cl}$ (Å)	% dev[b]
RI-MP2	6-31G(d,p)	1.014	1.041	2.111	3.123	0.7%
	6-31+G(d)	1.022	1.055	2.013	3.058	−1.4%
	6-311++G(2df,2p)	1.018	1.052	2.091	3.122	0.7%
	aug-cc-pVTZ	1.014	1.043	2.079	3.101	
B3LYP	6-31G(d,p)	1.018	1.050	2.112	3.136	1.1%
	6-31+G(d)[a]	1.021	1.050	2.142	3.165	2.1%
	6-311++G(2df,2p)	1.014	1.046	2.112	3.136	1.1%
	aug-cc-pVTZ	1.015	1.046	2.114	3.140	1.3%
M06-2X	6-31G(d,p)	1.017	1.048	2.081	3.105	0.1%
	6-31+G(d)	1.020	1.045	2.115	3.137	1.2%
	6-311++G(2df,2p)	1.014	1.041	2.111	3.124	0.7%
	aug-cc-pVTZ	1.014	1.044	2.087	3.113	0.4%

[a] Reference 15. [b] Percent deviation of $r_{N\cdots Cl}$ from the MP2/6-311++G(2df,2p) value. See Table 2 for definitions of notation used.

deviation from the RI-MP2 result, but B3LYP performs less well with deviations of 1% or greater irrespective of the basis set used. Because M06-2X/6-31G(d,p) calculations yielded acceptable geometries for all of the basis sets considered, this method was employed throughout the rest of the study. Analogous B3LYP calculations are also presented for purposes of comparison.

The geometries of the $(NH_4Cl)_n$, $NH_4^+(NH_4Cl)_n$, and $Cl^-(NH_4Cl)_n$ cluster systems are summarized in Figures 2, 3, and 4 respectively, using a graphical motif suggested by Martin.[53] The spiral is meant to connote the addition of a monomer unit to each cluster to form the next cluster in the sequence, although this may or may not be important in the actual mechanism for cluster formation. A number of reactions that may be relevant to cluster growth are considered later in this section.

Figure 2 illustrates the reaction series:

$$(NH_3\text{---}HCl) + (NH_4Cl)_n \rightarrow (NH_4Cl)_{n+1} \qquad (R1)$$

The structures of the $n > 10$ clusters are reported here for the first time. The M06-2X and B3LYP cluster geometries for the clusters with $n = 2-10$ are in substantial agreement with those predicted in previous work, where it was reported that even-numbered clusters tended to exhibit "slablike" structures and odd-numbered clusters tended to exhibit more compact structures.[14] One notable exception occurred in the case of $[(NH_4Cl)_7]$. In this case, geometry optimization of the globally minimum-energy structure of the cluster located by simulated annealing of the model potential produces a structure that is a saddle point at the DFT level, independent of the chosen functional. Repeated MW-SA calculations also indicated the presence of a "slablike" minimum-energy structure for $n = 7$, which was 4.7 kcal/mol higher in energy and which resembles the $n = 6$ structure with an ion pair attached to one edge. This structure continues to be a minimum-energy geometry after DFT geometry optimization and is presumed hereafter to be the true global minimum of the cluster. As observed previously, even-numbered clusters generally continue to have slablike structures

dx.doi.org/10.1021/jp2069732 |J. Phys. Chem. A 2011, 115, 10423–10432

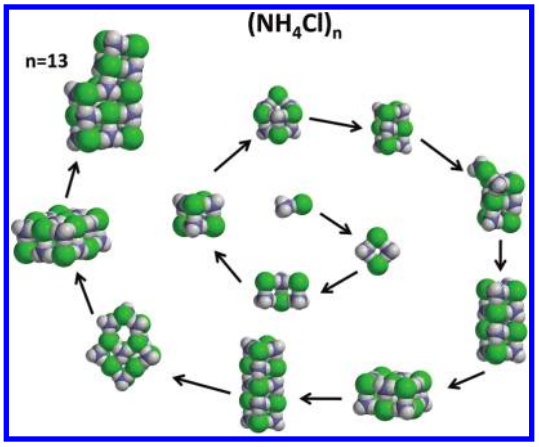

Figure 2. Structures of $(NH_4Cl)_n$ clusters obtained using "mag-walk" simulated annealing and subsequent M06-2X/6-31G(d,p) geometry optimization. The central cluster in the image corresponds to the hydrogen-bonded $NH_3\cdots HCl$ system, while all larger clusters consist of interacting NH_4^+ and Cl^- ions.

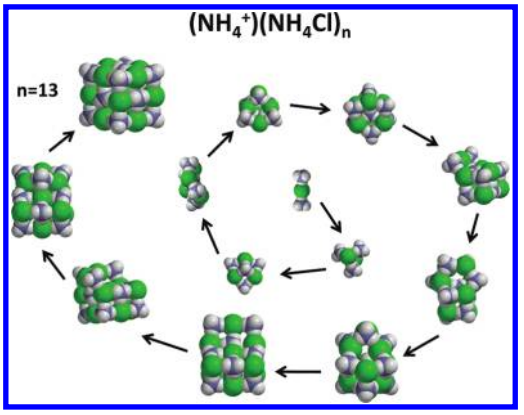

Figure 3. Geometries of $(NH_4^+)(NH_4Cl)_n$ clusters obtained using "mag-walk" simulated annealing and subsequent M06-2X/6-31G(d,p) geometry optimization. Here, the central cluster in the image consists of the $(NH_4^+)(NH_4Cl)$ species.

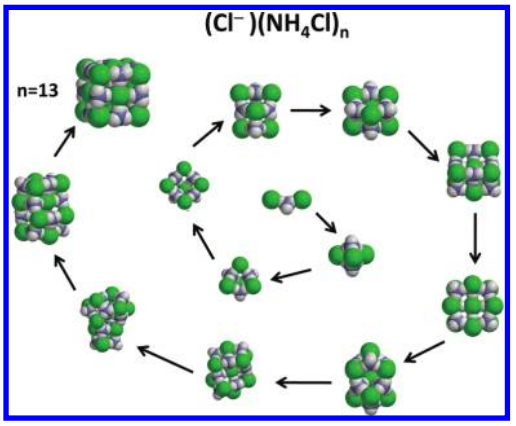

Figure 4. Geometries of $Cl^-(NH_4Cl)_n$ clusters obtained using "mag-walk" simulated annealing and subsequent M06-2X/6-31G(d,p) geometry optimization.

and odd-numbered clusters are more compact, with the exception of the $n = 7$ and $n = 13$ clusters, which are also slablike.

The cation cluster sequence depicted in Figure 3 corresponds to the reaction:

$$(NH_3\text{---}HCl) + (NH_4^+)(NH_4Cl)_n \rightarrow (NH_4^+)(NH_4Cl)_{n+1} \quad (R2)$$

All of these clusters, as well as the anion clusters, are presented for the first time in the present work. In some cases ($n = 4, 5, 6, 13$), these clusters have geometries similar to the $Na^+(NaCl)_n$ cluster geometries presented by Martin.[53] For both the sodium and the ammonium chlorides, the $n = 13$ cluster is a cubic "rocksalt" structure with alternating cations and anions along each edge and through the interior. The $n = 4$ clusters for both systems are "bowl-shaped", and the $n = 5, 6$ clusters are compact in both cases. The monomer clusters are also similar in that both have a central anion; however, $(NH_4^+)(NH_4Cl)$ is linear, whereas $(Na^+)(NaCl)$ is bent. For $n = 2$, the cation cluster is a compact structure with each chloride coordinated to three ammonium cations, whereas the $(Na^+)(NaCl)_2$ cation is a bent chain of alternating cations and anions with each chloride coordinated to only two sodium cations. The $n = 7$ ammonium chloride cation cluster is shaped somewhat like an "easy chair", whereas the $Na^+(NaCl)_7$ cluster has a C_2 axis containing a mirror plane of symmetry.

In Figure 4, the anion cluster sequence shown in Figure 3 illustrates the reaction:

$$(NH_3\text{---}HCl) + (Cl^-)(NH_4Cl)_n \rightarrow (Cl^-)(NH_4Cl)_{n+1} \quad (R3)$$

The $n = 1$ anion cluster is nonlinear, with a central NH_4^+ coordinated with each of the two Cl^- ions. In the case of $n = 2$, the anion structure has terminal ammonium ions, with each ammonium coordinated to three chloride anions. For $n = 13$, the anion cluster geometry strongly resembles that of the cation ammonium chloride cluster, with cations and anions replacing one another throughout the cluster. The $n = 3$ geometries of the cation and anion clusters also have close correspondence with one another. However, no such simple replacement correlates the other anion and cation geometries of ammonium chloride. Note for example that the $n = 10$ anion cluster is a relatively compact structure, whereas the $n = 10$ cation cluster is more "slablike".

Following Matro et al.,[14] we predict the relative stabilities of the clusters in each sequence by calculating V_n, the interaction energy of the nth cluster as compared to its component gas-phase ions, and plotting $\Delta V_n = V_{n-1} - V_n$, which is the gain in interaction energy for the nth cluster. In the case of the neutral clusters, there is no ambiguity when we consider only clusters with $n > 1$. Although the neutral monomer does not consist of an ion pair, we still define the interaction energy relative to the gas-phase ions for consistency. In the case of the neutral clusters, V_n^0 is the difference of the electronic energies of products and reactants for the reaction R4:

$$n(NH_4^+) + n(Cl^-) \rightarrow (NH_4Cl)_n \quad (R4)$$

The interaction energy of the cation clusters, V_n^+, is obtained from the reaction R5:

$$(n + 1)(NH_4^+) + n(Cl^-) \rightarrow (NH_4^+)(NH_4Cl)_n \quad (R5)$$

Table 4. Interaction Energies per Ion Pair for Neutral, Cation, and Anion Clusters[a]

n	V_n^+/n	V_n^0/n	V_n^-/n
1	−523.1 (−523.2)	−560.2	−693.8
2	−543.2 (−542.7)	−613.0	−702.5
3	−558.6 (−558.2)	−625.7	−699.3
4	−557.3 (−557.0)	−656.6	−690.4
5	−562.7 (−562.1)	−652.8	−694.9
6	−569.5 (−568.5)	−664.6	−699.7
7	−564.0	−659.7	−691.7
8	−567.6	−670.4	−694.8
9	−566.6	−671.4	−695.7
10	−565.8	−673.3	−692.3
11	−564.8	−671.8	−693.8
12	−567.8	−677.7	−695.0
13	−570.8	−675.3	−695.2

[a] Energies in kJ/mol. Interaction energies are calculated at the M06-2X/6-311G++(2df,2p)//M06-2X/6-31G(d,p) level of theory. Numbers in parentheses are calculated at the M06-2X/aug-cc-pVTZ level of theory.

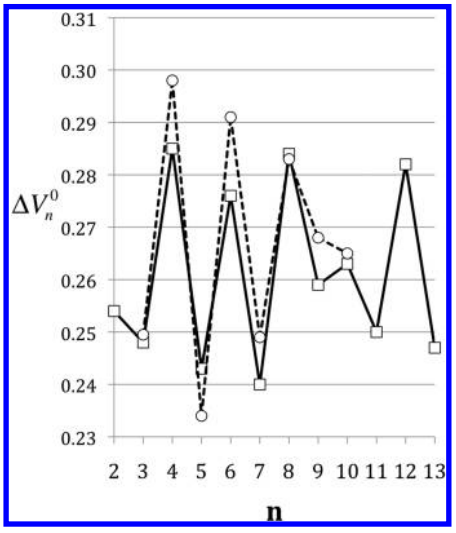

Figure 5. ΔV_n^0 (hartree) for $(NH_4Cl)_n$ clusters, calculated from M06-2X/6-311G++(2df,2p) single-point energies (○) of geometries shown in Figure 2. Also shown is ΔV_n^0 from ref 14 calculated using the same empirical model employed in the mag-walking simulated annealing calculations (□). See text for definition of ΔV_n^0.

whereas the interaction energy of the anion clusters, defined as V_n^-, corresponds to the reaction R6:

$$n(NH_4^+) + (n+1)(Cl^-) \rightarrow (Cl^-)(NH_4Cl)_n \qquad (R6)$$

The interaction energies for all three cluster types per ion pair are summarized in Table 4.

The stability trends of the neutral clusters are depicted in Figure 5, which shows the behavior of ΔV_n^0 as a function of n in comparison to previous work by Matro et al.[14] The agreement is remarkably good between two completely different methods of computation (M06-2X vs an empirical force model). In both cases, we see a notable alternation in stability between even and odd values of n, with much less stabilization for n = 10 as compared to the other even-numbered clusters. However, the M06-2X calculations predict that the n = 8 cluster has a gain in

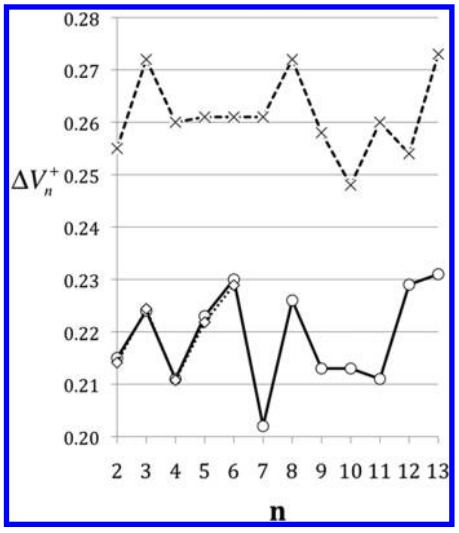

Figure 6. ΔV_n^+ (hartree) for $(NH_4^+)(NH_4Cl)_n$ clusters, calculated from M06-2X/6-311G++(2df,2p)//6-31G(d,p) energies (○) of geometries shown in Figure 3. Also shown is ΔV_n^+ calculated from M06-2X/aug-cc-pVTZ energies (◇) and B3LYP/6-311G++(2df,2p)//6-31G(d,p) energies (×).

interaction energy equal to that of n = 4, whereas the interaction potential used by Matro et al. predicted that the peaks of the even-numbered clusters decreased in size from 4 to 8. The M06-2X calculations also show that the n = 10 cluster has a small maximum in the ΔV_n^0 plot, whereas previous work predicted that this cluster was not a maximum.

Once again following Matro et al., in Figure 6 a plot of ΔV_n^+ is provided using different basis sets and levels of theory. Single-point M06-2X energies calculated using the 6-311++G(2df,2p) basis set are seen to produce results that are nearly identical to those calculated using the (much more numerically intensive) aug-cc-pVTZ basis set; for this reason, the former basis is used throughout the rest of this Article. We see that the B3LYP and M06-2X methods both predict a local maximum in the interaction energy, and therefore enhanced stability, for the n = 3 cluster. This is in qualitative agreement with the anomalous TS-MS result.[12] However, the B3LYP calculation does not predict a particularly stable cation cluster at n = 6, whereas the M06-2X method predicts a maximum for both of the basis sets employed. The M06-2X method also predicts a steep increase in interaction energy for n = 4 to n = 6, in contrast to the B3LYP result. Thus, only the M06-2X predictions are in qualitative agreement with the second anomaly reported by Röllgren and co-workers.[12] Both the B3LYP and the M06-2X methods also show enhanced stability for the n = 13 cation cluster, another "magic number" in the TS-MS spectra.[13] However, both methods also display a maximum at n = 8, which does not appear to have a correspondingly enhanced peak in the TS mass spectra except at very low jet temperatures. One possible interpretation is that the n = 8 cation cluster is kinetically unstable at elevated temperature; that is, it may decompose to smaller fragments at high temperature but become thermodynamically favored at low temperature. If this point of view is adopted, then the trends in ΔV_n^+ provide a useful interpretive framework for the experimental results.

As noted previously, the anion clusters have not been considered in previous work. Figure 7 shows the changes in binding energy for the anion clusters by plotting ΔV_n^- as a function of n. The curve shows maximum values at n = 2, 6, 8 and a plateau at

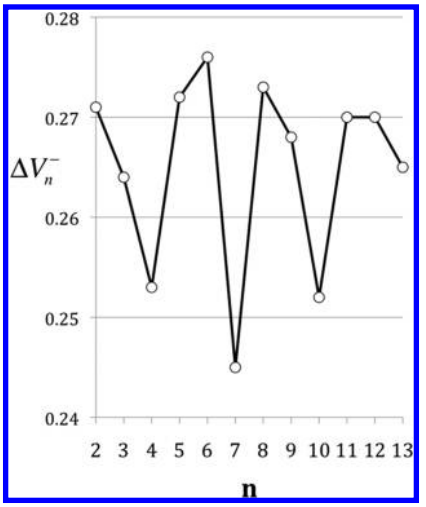

Figure 7. ΔV_n^- (hartree) for $Cl^-(NH_4Cl)_n$ clusters, calculated from M06-2X/6-311G++(2df,2p)//M06-2X/6-31G(d,p) energies (○) of geometries shown in Figure 4.

Table 5. ΔH^0 and ΔG^0 for Vapor-Phase Cluster Growth Reactions R1, R2, and R3[a]

	neutral		cation		anion	
n	$\Delta_1 H^0$	$\Delta_1 G^0$	$\Delta_2 H^0$	$\Delta_2 G^0$	$\Delta_3 H^0$	$\Delta_3 G^0$
1			−135	−98	−131	−97
2	−87	−35	−114	−58	−135	−82
3	−77	−30	−129	−84	−120	−72
4	−172	−114	−93	−48	−92	−53
5	−63	−12	−135	−79	−136	−72
6	−150	−102	−161	−98	−145	−91
7	−57	−18	−65	−25	−72	−30
8	−168	−111	−139	−88	−142	−85
9	−102	−52	−109	−52	−126	−66
10	−118	−65	−94	−53	−89	−43
11	−79	−21	−105	−49	−132	−74
12	−149	−81	−152	−95	−134	−82
13	−89	−56	−158	−102	−110	−75

[a] Energies in kJ/mol. Geometries, frequencies, and associated thermodynamic quantities except for electronic energies are calculated for reactions R1, R2, and R3 at the M06-2X/6-31G(d,p) level; electronic energies are calculated at the M06-2X/6-311G++(2df,2p)//M06-2X/6-31G(d,p) level.

n = 11, 12. Notably, the n = 13 cluster does not appear to be favored. It would be extremely interesting to compare the abundances implied by these curves to experimental TS-MS data for the negative ions, but apparently there is no such data available in the literature. TOF mass spectra of $Cl^-[NaCl]_n$ and $Cl^-[CsCl]_n$ clusters generated by laser vaporization of solids have been obtained.[54] In that work, both systems were observed to exhibit enhanced intensity at n = 4 and 13, in contrast to the present findings for the ammonium chloride clusters.

To provide data that may be relevant to the nucleation and growth of small ammonium chloride particles under dry conditions, we consider reactions in which the particle size increases. Accordingly, the predicted enthalpies and free energies of reaction

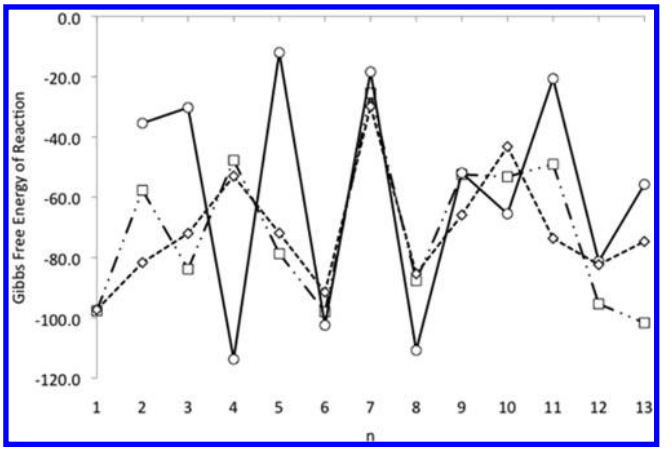

Figure 8. Free energies of reaction (kJ/mol) for cluster growth reactions R4, R5, and R6 by monomer addition to form the cation (□), neutral (○), or anion (◇) cluster as a function of cluster size.

Table 6. ΔH^0 and ΔG^0 for Vapor-Phase Cluster Growth Reactions R7 and R8[a]

	cation		anion	
n	$\Delta_7 H^0$	$\Delta_7 G^0$	$\Delta_8 H^0$	$\Delta_8 G^0$
1	−135	−98	−131	−97
2	−162	−120	−179	−144
3	−214	−173	−222	−185
4	−134	−107	−141	−125
5	−207	−174	−214	−184
6	−218	−170	−210	−173
7	−227	−177	−225	−185
8	−198	−154	−199	−160
9	−205	−154	−224	−173
10	−182	−142	−196	−151
11	−209	−170	−249	−204
12	−212	−184	−233	−205
13	−281	−230	−255	−224

[a] Energies in kJ/mol. See the footnote of Table 5 for a summary of the methods used.

for reactions R1−R3 are calculated under standard conditions (P = 1 atm, T = 298 K) within the rigid-rotator/harmonic oscillator approximation (Table 5). Free energies of reaction for these reactions using M06-2X/6-31G(d,p) geometries and harmonic frequencies and M06-2X/6-311++G(2df,2p) single-point energies are shown as a function of n in Figure 8. The strong n-dependence of all three curves is striking and generally shows minima at the same values of n, which maximize the interaction energies.

Another possible contribution to the nucleation and growth of particles is the attachment of an ion to a neutral cluster. Table 6 gives the predicted enthalpies, entropies, and free energies of reaction for the formation of the cation and anion clusters by such an addition, that is, reactions R7 and R8:

$$NH_4^+ + (NH_4Cl)_n \rightarrow (NH_4^+)(NH_4Cl)_n \quad (R7)$$

$$Cl^- + (NH_4Cl)_n \rightarrow (Cl^-)(NH_4Cl)_n \quad (R8)$$

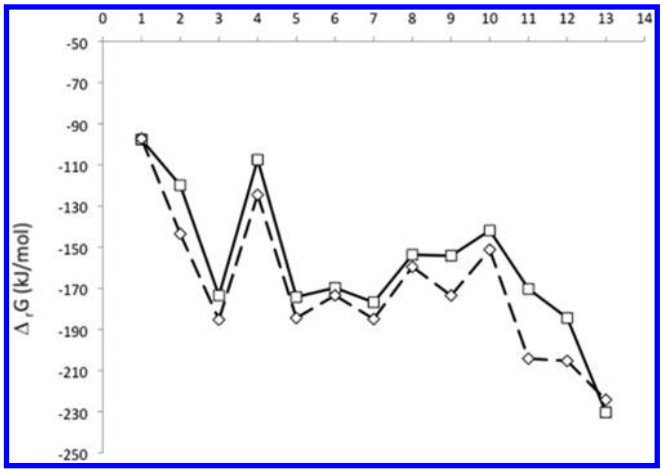

Figure 9. Free energies of reaction (kJ/mol) for ion formation by attachment of an ion to a neutral cluster as a function of cluster size; see reactions R7 (square) and R8 (diamond).

Figure 9 shows the dependence of the free energies of reaction for these two reactions on the size of the clusters. The general trend is for the reactions to become more exergonic as the size of the cluster increases, with notable exceptions at $n = 4$ and $n = 10$.

CONCLUSIONS

The cluster geometries predicted by the MW-SA method agree perfectly with those obtained previously for the $(NH_4Cl)_n$, $n = 2-10$, clusters using Brownian dynamics simulated annealing and parallel jump-walking calculations. The good qualitative agreement of the gain in interaction energy of the cation clusters with the stabilities inferred from thermospray mass spectrometry is fairly satisfying. In one case ($n = 8$), a local maximum in stabilization is predicted, which does not appear to match the TS-MS magic number distribution. It is possible that the octomer cation cluster is kinetically favored to decompose to a smaller cluster at the TS-MS conditions (near 350 K), which would also explain the substantial enhancement of the $n = 8$ peak that occurs as the temperature is lowered. Further work should be carried out to confirm or deny this. The results would predict that TS-MS spectra of the anion clusters would display "magic numbers" at $n = 2$, 6, 8, but no evidence is seen for $n = 13$ to be a magic number for the anion cluster. This is in contrast to what has been observed experimentally for negatively charged alkali halide clusters.[54]

Only one of the clusters studied here, whether neutral or charged, exhibited conformational changes during geometry optimization. Moreover, only the neutral monomer cluster consisted of recognizable ammonia and hydrogen chloride molecules. In every other cluster system considered here, no evidence of proton transfer from ammonium to chloride was observed. This information may be relevant to the development of force fields for molecular dynamics simulations of ionic liquids.[55]

As noted previously, a derivative compound of the neutral tetramer has been synthesized.[4] The current calculations predict that the $n = 6$ and $n = 8$ neutral clusters are even more stable than the tetramer. It may be possible to synthesize derivatives of the larger clusters as well. As the current calculations do not include water molecules, they are insufficient for modeling the thermodynamics of cluster growth or the corrosivity of ammonium chloride nanoparticles under atmospheric conditions. However, the inclusion of water molecules in MW-SA calculations appears to be straightforward and is planned for future work.

ASSOCIATED CONTENT

Supporting Information. Coordinates in *xyz* format for M06-2X/6-31G(d,p) geometries of all of the molecules and clusters presented in this work. This material is available free of charge via the Internet at http://pubs.acs.org.

AUTHOR INFORMATION

Corresponding Author

*Phone: (212) 353-4378. Fax: (212) 353-4341. E-mail: topper@cooper.edu.

Present Addresses

[§]Department of Physics and Engineering Physics, Stevens Institute of Technology, Castle Point on Hudson, Hoboken, New Jersey 07030, United States.

[∥]Department of Materials Science and Engineering, University of California — Berkeley, 210 Hearst Memorial Mining Building, Berkeley, California 94720-1760, United States.

ACKNOWLEDGMENT

Partial support for this work was provided by grants from the U.S. Army through the Academy of Applied Sciences' REAP program and from Merck, Inc. through a Merck-SURF grant. We would like to acknowledge Jodie Mueller and Eugene Agichtein (Cooper Union) and Grace Lee and Katherine Russamano (Monmouth University) for their contributions to early stages of this project.

REFERENCES

(1) Martin, T. P. *Phys. Rep.* **1983**, *95*, 167–199.
(2) Baker, A. D.; Baker, M. D. *J. Phys. Chem. C* **2009**, *113*, 14793–14797.
(3) Sun, S.; Zheng, Q.; Wen, J.; Li, D. *Mater. Corros.* **2010**, *10*, 852–859.
(4) Schulenberg, N.; Hübner, O.; Kaifer, E.; Himmel, H.-J. *Eur. J. Inorg. Chem.* **2008**, *2008*, 2165–2169.
(5) Behera, S. N.; Sharma, M. *Sci. Total Environ.* **2010**, *408*, 3569–3575.
(6) Harrison, R. M.; Pio, C. A. *Atmos. Environ.* **1983**, *17*, 1733–1738.
(7) Lewis, E. R.; Schwartz, S. E. *Sea Salt Aerosol Production: Mechanisms, Methods, Measurements and Models*; American Geophysical Union: Washington, DC, 2004.
(8) Wexler, A. S.; Seinfeld, J. H. *Atmos. Environ., Part A* **1990**, *24*, 1231–1246.
(9) Bai, H.; Lu, C.; Ling, Y. M. *Atmos. Environ.* **1995**, *29*, 313–321.
(10) Korhonen, P.; Kulmala, M.; Viisanen, Y. *J. Aerosol Sci.* **1997**, *28*, 901–917.
(11) Keck, L.; Wittmaack, K. *Atmos. Environ.* **2005**, *39*, 4093–4100.
(12) Schmelzeisen-Redeker, G.; Wong, S. S.; Giessmann, U.; Röllgren, F. W. *Z. Naturforsch.* **1985**, 430–431.
(13) Nehring, H.; Thiebes, S.; Bütfering, L.; Röllgren, F. W. *Int. J. Mass Spectrom. Ion Processes* **1993**, *128*, 123–132.
(14) Matro, A.; Freeman, D. L.; Topper, R. Q. *J. Chem. Phys.* **1995**, *104*, 8690–8702.
(15) Tao, F.-M. *J. Chem. Phys.* **1999**, *110*, 11121–11124.
(16) Stevenson, R. *J. Chem. Phys.* **1961**, *34*, 1757–1762.
(17) Wagner, E. L.; Hornig, D. F. *J. Chem. Phys.* **1949**, *17*, 105.
(18) Topper, R. Q.; Freeman, D. L. *Los Alamos Chemical Physics Preprint Database*, No. 9403002, 1994; http://arxiv.org/abs/chem-ph/9403002.

(19) Parsonage, N. G.; Staveley, L. A. K. *Disorder in Crystals*; Clarendon Press: Oxford, UK, 1978.
(20) Cerjan, C. J.; Miller, W. H. *J. Chem. Phys.* **1981**, *75*, 280.
(21) Simons, J.; Jorgensen, P.; Taylor, H.; Ozment, J. *J. Phys. Chem.* **1985**, *89*, 52.
(22) Goodwin, E. J.; Howard, N. W.; Legon, A. C. *Chem. Phys. Lett.* **1986**, *131*, 319.
(23) Chaban, G. M.; Gerber, R. B.; Janda, K. J. *J. Phys. Chem. A* **2001**, *105*, 8323–8332.
(24) Biczysko, M.; Latajka, Z. *J. Chem. Phys.* **1999**, *313*, 366.
(25) Del Bene, J. E.; Jordan, M. J. T. *J. Chem. Phys.* **1998**, *108*, 3205.
(26) Jordan, M. J. T.; Del Bene, J. E. *J. Am. Chem. Soc.* **2000**, *122*, 2101.
(27) Alavi, S.; Thompson, D. L. *J. Chem. Phys.* **2002**, *117*, 2599–2608.
(28) Biczysko, M.; Latajka, Z. *J. Phys. Chem. A* **2002**, *106*, 3197–3201.
(29) Eustis, S. N.; Radisic, D.; Bowen, K. H.; Bachorz, R. A.; Haranczyk, M.; Schenter, G. K.; Gutowski, M. *Science* **2008**, *319*, 936–939.
(30) Biczysko, M.; Latajka, Z. *Chem. Phys. Lett.* **1999**, *313*, 366–373.
(31) Asada, T.; Takitani, S.; Koseki, S. *J. Phys. Chem. A* **2005**, *109*, 1821–1827.
(32) Li, R.-J.; Li, Z.-R.; Wu, D.; Hao, X.-Y.; Li, Y.; Wang, B.-Q.; Tao, F.-M.; Sun, C.-C. *Chem. Phys. Lett.* **2003**, *372*, 893–898.
(33) Lee, C.; Yang, W.; Parr, R. G. *Phys. Rev. B* **1988**, *37*, 785–789.
(34) Becke, A. D. *J. Chem. Phys.* **1993**, *98*, 5648–5652.
(35) Zhao, Y.; Truhlar, D. G. *Theor. Chem. Acc.* **2008**, *120*, 215–241.
(36) Zhao, Y.; Truhlar, D. G. *Acc. Chem. Res.* **2008**, *41*, 157–167.
(37) Wales, D. J. *Energy Landscapes: Applications to Clusters, Biomolecules and Glasses*; Cambridge University Press: Cambridge, UK, 2004.
(38) Topper, R. Q.; Freeman, D. L.; Bergin, D.; LaMarche, K. In *Reviews in Computational Chemistry*; Lipkowitz, K. B., Larter, R., Cundari, T. R., Eds.; Wiley-VCH/John Wiley and Sons: New York, 2003; Vol. 19, pp 1−41.
(39) Frantz, D. D.; Freeman, D. L.; Doll, J. D. *J. Chem. Phys.* **1990**, *93*, 2769.
(40) Metropolis, N.; Rosenbluth, A.; Rosenbluth, M. N.; Teller, A.; Teller, E. *J. Chem. Phys.* **1953**, *21*, 1087.
(41) Barker, J. A.; Watts, R. O. *Chem. Phys. Lett.* **1969**, *3*, 144.
(42) Kirkpatrick, S.; Gelatt, C. D.; Vecchi, M. P. *Science* **1983**, *220*, 671–680.
(43) Torres, F. M.; Agichtein, E.; Grinberg, L.; Yu, G.; Topper, R. Q. *J. Mol. Struct. (THEOCHEM)* **1997**, *419*, 85.
(44) Lee, J. K.; Barker, J. A.; Abraham, F. F. *J. Chem. Phys.* **1973**, *58*, 3166.
(45) Clark, T.; Chandrasekhar, J. *J. Comput. Chem.* **1983**, *4*, 294–301.
(46) Vahtras, O.; Almlof, J.; Feyereisen, M. W. *Chem. Phys. Lett.* **1993**, *213*, 514.
(47) Woon, D. E.; Dunning, T. H. *J. Chem. Phys.* **1993**, *98*, 1358.
(48) Zhao, Y.; Truhlar, D. G. *J. Phys. Chem. A* **2005**, *109*, 6624–6627.
(49) Papjak, E.; Leverentz, H. R.; Zheng, J.; Truhlar, D. G. *J. Chem. Theory Comput.* **2009**, *5*, 1197–1202.
(50) Gordon, M. S.; Schmidt, M. W. In *Theory and Applications of Computational Chemistry: The First Forty Years*; Dykstra, C. E., Frenking, G., Kim, K. S., Scuseria, G. E., Eds.; Elsevier: Amsterdam, 2005; pp 1167−1189.
(51) Shao, Y.; Molnar, L. F.; Jung, Y.; Kussmann, J.; Ochsenfeld, C.; Brown, S. T.; Gilbert, A. T. B.; Slipchenko, L. V.; Levchenko, S. V.; O'Neill, D. P.; DiStasio, R. A., Jr.; Lochan, R. C.; Wang, T.; Beran, G. J. O.; Besley, N. A.; Herbert, J. M.; Lin, C. Y.; Van Voorhis, T.; Chien, S. H.; Sodt, A.; Steele, R. P.; Rassolov, V. A.; Maslen, P. E.; Korambath, P. P.; Adamson, R. D.; Austin, B.; Baker, J.; Byrd, E. F. C.; Dachsel, H.; Doerksen, R. J.; Dreuw, A.; Dunietz, B. D.; Dutoi, A. D.; Furlani, T. R.; Gwaltney, S. R.; Heyden, A.; Hirata, S.; Hsu, C.-P.; Kedziora, G.; Khalliulin, R. Z.; Klunzinger, P.; Lee, A. M.; Lee, M. S.; Liang, W. Z.; Lotan, I.; Nair, N.; Peters, B.; Proynov, E. I.; Pieniazek, P. A.; Rhee, Y. M.; Ritchie, J.; Rosta, E.; Sherrill, C. D.; Simmonett, A. C.; Subotnik, J. E.; Woodcock, H. L., III; Zhang, W.; Bell, A. T.; Chakraborty, A. K.; Chipman, D. M.; Keil, F. J.; Warshel, A.; Hehre, W. J.; Schaefer, H. F.; Kong, J.; Krylov, A. I.; Gill, P. M. W.; Head-Gordon, M. *Phys. Chem. Chem. Phys.* **2006**, *8*, 3172.
(52) Goodwin, E. J.; Howard, N. W.; Legon, A. C. *Chem. Phys. Lett.* **1986**, *131*, 319.
(53) Martin, T. P. In *Elemental and Molecular Clusters*; Benedek, G., Martin, T. P., Paccioni, G., Eds.; Springer Series in Materials Science; Springer: Berlin, 1988; Vol. 6, pp 2−9;
(54) Twu, Y. J.; Conover, C. W. S.; Yang, Y. A.; Bloomfield, L. A. *Phys. Rev. B* **1990**, *42*, 5306–5316.
(55) Guillot, B.; Guissani, Y. *J. Chem. Phys.* **2002**, *116*, 2047–2057.